Sources, Sinks, and the Distribution of OH in the Lower Stratosphere†

T. F. Hanisco,*,‡ E. J. Lanzendorf,‡ P. O. Wennberg,§ K. K. Perkins,‡ R. M. Stimpfle,‡ P. B. Voss,‡ J. G. Anderson,‡ R. C. Cohen,⊥ D. W. Fahey,|| R. S. Gao,|| E. J. Hintsa,¶ R. J. Salawitch,# J. J. Margitan,# C. T. McElroy,▽ and C. Midwinter▽

Department of Chemistry, Harvard University, 12 Oxford Street, Cambridge, Massachusetts 02138, California Institute of Technology, Pasadena, California, University of California, Berkeley, California, NOAA Aeronomy Laboratory, National Oceanic and Atmospheric Administration, Boulder, Colorado, Woods Hole Oceanographic Institution, Woods Hole, Massachusetts, Jet Propulsion Laboratory, Pasadena, California, and Atmospheric Environment, Downsview, Ontario, Canada

Received: July 3, 2000; In Final Form: October 18, 2000

Extensive measurement campaigns by the NASA ER-2 research aircraft have obtained a nearly pole-to-pole database of the species that control HO_x ($OH + HO_2$) chemistry. The wide dynamic range of these in situ measurements provides an opportunity to demonstrate empirically the mechanisms that control the HO_x system. Measurements in the lower stratosphere show a remarkably tight correlation of OH concentration with the solar zenith angle (SZA). This correlation is nearly invariant over latitudes ranging from 70° S to 90° N and all seasons. An analysis of the production and loss of HO_x in terms of the rate determining steps of reaction sequences developed by Johnston and Podolske and Johnston and Kinnison is used to clarify the behavior of the system and to directly test our understanding of the system with observations. Calculations using in situ measurements show that the production rate of HO_x is proportional to O_3 and ultraviolet radiation flux. The loss rate is proportional to the concentration and the partitioning of NO_y (reactive nitrogen) and the concentration of HO_2. In the absence of heterogeneous reactions, the partitioning of NO_y is controlled by O_3 and HO_x and the concentration of HO_2 is controlled by NO_y and O_3, so that the removal rate of OH is buffered against changes in the correlation of O_3 and NO_y. The heterogeneous conversion of NO_2 to HNO_3 is not an important net source of HO_x because production and removal sequences are nearly balanced. Changes in NO_y partitioning resulting from heterogeneous chemistry have a large effect on the loss rates of HO_x, but little or no impact on the measured abundance of OH. The enhanced loss rates at high NO_2/HNO_3 are offset in the data set examined here by enhanced production rates resulting from increased photolysis rates resulting from the decreased O_3 column above the ER-2.

Introduction

The hydroxyl radical (OH) plays a central role in the photochemistry that controls the O_3 in the lower stratosphere. OH is involved directly in the hydrogen radical controlled reaction sequences that are the dominant mechanism for the removal of O_3 in the mid-latitude lower stratosphere.[1] OH plays an additional role by altering the partitioning of the nitrogen and halogen chemical families that control O_3 removal in the high latitude summer and winter, respectively.[2−4] Because OH is involved in such a large number of photochemical processes, the expectation is that the concentration of OH would show substantial variability depending on the state of the atmosphere. In fact, we find that the concentration of OH is nearly independent of all photochemical parameters except the O_3 slant column, which is a function of the solar zenith angle (SZA) and column O_3 above the aircraft. Surprisingly, the concentration of OH is the most predictable of the radicals in the lower stratosphere (see Figure 1). Because of this fact, the concentration of OH in most of the lower stratosphere can be accurately parametrized as a function of SZA. Such parametrizations have been used extensively in the analysis of the photochemistry of the lower stratosphere.[1−2,5−7] In this analysis we examine why the concentration of OH is to first order a simple function of SZA.

While OH and the hydroperoxy radical (HO_2) are tightly coupled through fast photochemical reactions, the HO_x ($OH + HO_2$) system exhibits specific simplifying characteristics. Generally, the partitioning between OH and HO_2 occurs on a much faster time scale than the production and loss of HO_x, allowing these processes to be treated separately analytically. In addition, the production and loss of HO_x occurs primarily through OH, so that the production/loss of OH and the production/loss of HO_x are nearly synonymous. Thus it is straightforward to examine the production and loss of HO_x using measurements of OH. Furthermore, the photochemistry that controls HO_x is fast, so that a large number of intermediates in the reactions that produce and remove HO_x are in steady state. This enables an analysis of the production and loss processes of HO_x in terms of the rate determining steps of reaction sequences described by Johnston and Podolske and Johnston and Kinnison.[8,9] This approach reduces the system to a small number of net sources and sinks and dramatically clarifies the behavior of the system

† Part of the special issue "Harold Johnston Festschrift".

* Corresponding author. Phone: 617-495-5922. Fax: 617-495-4902. E-mail: tfh@huarp.harvard.edu.

‡ Harvard University.

§ California Institute of Technology.

⊥ University of California.

|| NOAA Aeronomy Laboratory.

¶ Woods Hole Oceanographic Institution.

Jet Propulsion Laboratory.

▽ Atmospheric Environment.

10.1021/jp002334g CCC: $20.00
Published on Web 12/21/2000

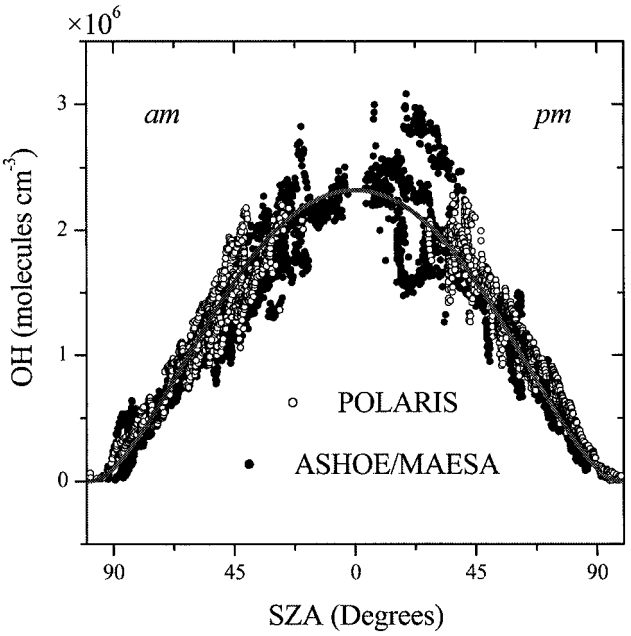

Figure 1. In situ measurements of OH obtained during ASHOE/MAESA and POLARIS versus the solar zenith angle (SZA). The data are restricted to $M < 2.5 \times 10^{18}$ molecules cm^{-3} and averaged into 1 min bins. The line is a fit to the data using a linear combination of secant functions used to parametrize the photolysis rates of O_3 and H_2CO.

and enhances our ability to directly test the system with observations.

We present measurements of OH and other species obtained by instruments flown aboard the NASA ER-2 high-altitude research aircraft. The wide dynamic range of atmospheric conditions sampled by these measurements provides an opportunity to gain insight into the mechanisms that control the HO_x system. In this analysis, in situ measurements are used along with photolysis rates determined from in situ measurements of overhead column O_3 to calculate the production and loss rates that govern the concentration of OH under a variety of atmospheric conditions. The results of these calculations are used to show how production and loss rates of HO_x are correlated and why concentrations of OH are buffered from changes in individual sources or sinks of HO_x within this data set.

Measurements

The measurements presented here were obtained aboard the NASA ER-2 during two extensive campaigns: the 1994 Airborne Southern Hemisphere Ozone Experiment/Measurements for Assessing the Effects of Stratospheric Aircraft (ASHOE/MAESA) deployed primarily in Christchurch, New Zealand (43° S, 173° W) and the 1997 Polar Ozone Loss in the Summer (POLARIS) deployed in Fairbanks, Alaska (65° N, 148° W).[10,11] The aircraft payload included instruments measuring most of the species necessary to test the chemistry of HO_x: OH, HO_2, NO, NO_2, NO_y (the sum of reactive nitrogen: $NO_x + HNO_3 + HNO_4 + ClONO_2 + 2N_2O_5$ ...), ClO, H_2O, O_3, CH_4, CO, HCl, pressure, temperature, and spectrally resolved radiation fields.[11]

Figure 1 shows in situ measurements of OH obtained during ASHOE/MAESA and POLARIS plotted versus SZA. The data are restricted to $M < 2.5 \times 10^{18}$ molecules cm^{-3} (~17−21 km) and averaged into 1 min bins. As will be shown, the diurnal change of OH is controlled by the production of HO_x from

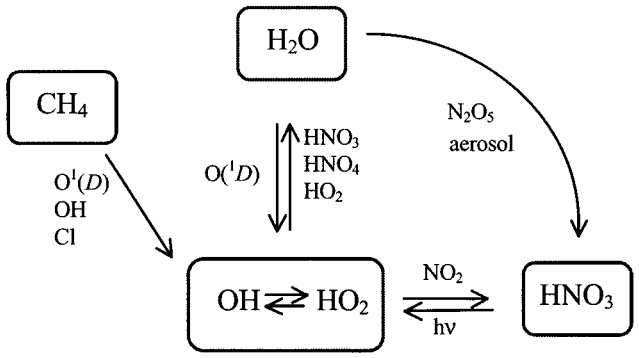

Figure 2. Primary sources and sinks of HO_x. Intermediate steps are not shown in the figure but are shown in equations in the text.

$O(^1D)$ and CH_2O. The line is a fit to the data using a linear combination of secant functions used to parametrize the photolysis rates of O_3 to produce $O(^1D)$ and of CH_2O to produce HCO:

$$J = J_0 \exp[-\zeta(\sec(\chi) - 1)]$$

$$J_1:\ J_0 = 8 \times 10^{-5},\quad \zeta = 2.2,\quad \chi = 0.85 \times \mathrm{SZA}$$

$$J_2:\ J_0 = 6.4 \times 10^{-5},\quad \zeta = 0.67,\quad \chi = 0.86 \times \mathrm{SZA}$$

$$f(\mathrm{SZA}) = c_1 J_1 + c_2 J_2 \qquad (1)$$

where $c_1 = 1.5 \times 10^{10}$ and $c_2 = 1.75 \times 10^{10}$ molecules cm^{-3} s. The standard deviation about the line, representing the mean for a given SZA, is ±23% for all data and ±15% for SZA < 70°. The measurement accuracy for OH is ±25% 2-σ, with an instrument precision of $\pm 1 \times 10^4$ molecules cm^{-3} (~1%) for the 1 min averaged data.[12] Much of the variability in the observed OH can be reproduced by using the calculated photolysis rates rather than parametrizations, i.e., $f(\mathrm{SZA}) = c_1 J_{O(^1D)} + c_2 J_{CH_2O}$. At high SZA the abundance of OH is more difficult to parametrize because the variation is larger, ±40% for data obtained at SZA > 70°. Interpretation of the measurements of OH at these SZA's is discussed elsewhere.[13]

Analysis

Sources and Sinks of HO_x. The primary sources and sinks of HO_x are diagrammed in Figure 2. These are the most significant individual reactions that participate in the sequences that result in net production or loss of HO_x. The reactions that interchange OH and HO_2 are significantly faster than any of these reactions, and the conversion of H to HO_2 can be considered instantaneous, so the production or removal of any hydrogen radical is equivalent. Less significant reactions are not shown; their absence does not impact the results presented here. Reactions that participate only in null sequences with respect to HO_x, such as the reactions that interconvert OH and HO_2, are not included. In some cases, the intermediates of the sequences are in steady state (i.e. *instantaneous* steady state not diurnal steady state), and only the rate determining steps are used to quantify the production/loss of HO_x through that sequence. For example, the oxidation of CH_4 falls into this category. In other cases, the intermediates are not in steady state and production/loss terms must be determined explicitly. All sequences with HNO_3 as an intermediate fall into this second category.

The primary source of HO_x in the lower stratosphere is the oxidation of H_2O by $O(^1D)$. $O(^1D)$ is generated from the

photolysis of O_3 primarily at wavelengths less than ~330 nm and is strongly dependent on the overhead O_3 column and SZA.

$$O_3 + h\nu \rightarrow O(^1D) + O_2$$
$$O(^1D) + H_2O \rightarrow 2OH \quad \text{(R1)}$$
$$\text{net: } O_3 + H_2O \rightarrow 2OH + O_2 \quad \text{(S1)}$$

The rate of production of HO_x by this sequence is equal to twice the rate of the rate determining step (R1). The rates of reactions will be denoted by $r_{A+B} = k_{A+B}[A][B]$; e.g., the rate of *R*1 is $r_{O(^1D)+H_2O}$. Additional production of HO_x results from the reaction of $O(^1D) + H_2$ in a sequence similar to S1 and from the oxidation of CH_4 initiated by $O(^1D)$:

$$O_3 + h\nu \rightarrow O(^1D) + O_2$$
$$O(^1D) + CH_4 \rightarrow CH_3 + OH \quad \text{(R2)}$$
$$CH_3 + O_2 \rightarrow CH_3O_2$$
$$CH_3O_2 + NO \rightarrow CH_3O + NO_2$$
$$NO_2 + h\nu \rightarrow NO + O$$
$$O + O_2 \rightarrow O_3$$
$$CH_3O + O_2 \rightarrow CH_2O + HO_2$$
$$\text{net: } CH_4 + 2O_2 \rightarrow OH + HO_2 + CH_2O \quad \text{(S2)}$$

The intermediates in this sequence are assumed to be in photochemical steady state. In addition, the branching of the intermediate steps is assumed to be unity. This assumption is valid in the lower stratosphere where the competing reaction of the methylperoxy radical, $CH_3O_2 + HO_2$, is not significant. In this data set, the rate of $CH_3O_2 + NO$ is at least 20 times greater than that of $CH_3O_2 + HO_2$.

The production of CH_2O can lead to additional HO_x production when the photolysis of CH_2O produces H atoms.

$$CH_2O + h\nu \rightarrow H + CHO \quad \text{(R3)}$$
$$H + O_2 \rightarrow HO_2$$
$$CHO + O_2 \rightarrow HO_2 + CO$$
$$\text{net: } CH_2O + O_2 \rightarrow 2HO_2 + CO \quad \text{(S3)}$$

An alternate pathway for the photolysis of CH_2O is the production of H_2 and CO. In the lower stratosphere, the quantum yield of this pathway is roughly twice that of R3, depending on UV flux and temperature. The branching ratio of this step is equal to $J_{H-CHO}/(J_{H-CHO} + J_{H_2-CO}) \cong 0.35$, where J_{H-CHO} and J_{H_2-CO} correspond to the photolysis rates of CH_2O to produce H + HCO and H_2 + CO, respectively. The net yield of HO_x from the oxidation of CH_4 initiated by $O(^1D)$, sequences 2 and 3, is about 2.7 HO_x per CH_4.

Oxidation of CH_4 is also initiated by analogous reactions of CH_4 with OH and Cl, but the yields for these sequences are smaller. In the case in which $OH + CH_4 \rightarrow CH_3 + H_2O$, one OH is consumed and no OH is produced. In the case in which $Cl + CH_4 \rightarrow CH_3 + HCl$, no OH is produced in the initiation step and one OH is lost through the subsequent reaction $OH + HCl \rightarrow H_2O + Cl$. In these sequences the yield of OH is zero,

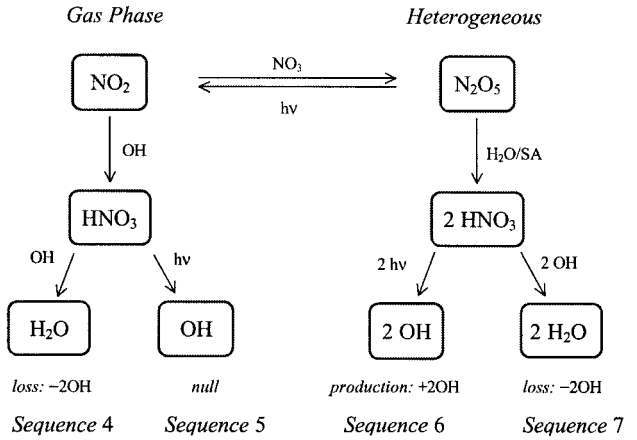

Figure 3. Gas-phase and heterogeneous sequences that involve HNO_3 as an intermediate. OH is produced or removed by the formation and subsequent removal of HNO_3.

but CH_2O is still produced, so that the net yield is roughly 0.7 HO_x per CH_4. Because CH_2O is in steady state, the production of HO_x through the combination of sequences 2 and 3, and the analogous sequences involving Cl and OH, is given by the rate of the initiation step multiplied by the yield of HO_x, e.g. $2.7\times r_{O(^1D)+CH_4}$, $0.7\times r_{OH+CH_4}$, and $0.7\times r_{Cl+CH_4}$, with the exact yields depending on UV flux and temperature. In the event that OH + HCl is not the primary sink of HCl, for example in the polar winter when the reaction of $HCl + ClONO_2$ is significant, the yield of OH from the chlorine initiated oxidation of methane is higher.

The primary net removal mechanism for HO_x is the reaction of NO_2 followed by reaction with HNO_3.

$$OH + NO_2 \xrightarrow{M} HNO_3 \quad \text{(R4)}$$
$$OH + HNO_3 \rightarrow H_2O + NO_3 \quad \text{(R5)}$$
$$NO_3 + h\nu \rightarrow NO_2 + O$$
$$\text{net: } 2OH \rightarrow H_2O + O \quad \text{(S4)}$$

In the limit in which HNO_3 is in steady state, the rate of this sequence is given by the rate of R5. In the middle and upper stratosphere this simplification is generally valid.[14] However, this condition is rarely met in the lower stratosphere due to the heterogeneous production and long lifetime of HNO_3. This and the competing sequences involving HNO_3 are diagrammed in Figure 3.

An alternate pathway is the reaction of NO_2 followed by photolysis of HNO_3 at wavelengths less than ~315 nm.

$$OH + NO_2 \xrightarrow{M} HNO_3 \quad \text{(R4)}$$
$$HNO_3 + h\nu \rightarrow OH + NO_2 \quad \text{(R6)}$$
$$\text{net: null} \quad \text{(S5)}$$

This sequence is a net null for OH, but it is used to determine the rates of the heterogeneous sequences below.

Heterogeneous reactions can convert H_2O to HO_x through the production of HNO_3 followed by photolysis. Likewise, the heterogeneous formation of HNO_3 followed by reaction with OH will remove HO_x.

$$\begin{aligned} &NO_2 + NO_3 \xrightarrow{M} N_2O_5 \\ &N_2O_5 + H_2O \xrightarrow{\text{aerosol}} 2HNO_3 \\ &2 \times (HNO_3 + h\nu \rightarrow OH + NO_2) \qquad \text{(R6)} \\ &NO_2 + O_3 \rightarrow NO_3 + O_2 \\ &\text{net: } H_2O + O_3 \rightarrow 2OH + O_2 \qquad \text{(S6)} \end{aligned}$$

$$\begin{aligned} &NO_2 + NO_3 \xrightarrow{M} N_2O_5 \\ &N_2O_5 + H_2O \xrightarrow{\text{aerosol}} 2HNO_3 \\ &2 \times (OH + HNO_3 \rightarrow H_2O + NO_3) \qquad \text{(R5)} \\ &NO_3 + h\nu \rightarrow NO_2 + O \\ &\text{net: } 2OH \rightarrow H_2O + O \qquad \text{(S7)} \end{aligned}$$

The concentration of NO_3 is negligible during the day; hence, N_2O_5 is produced only after the sun sets, and the heterogeneous production of HNO_3 occurs predominantly at night. As a result, the intermediates in these sequences are not in steady state and the production and loss of HO_x from reactions R6 and R5 must be determined explicitly. Because these reactions compete, the net effect of heterogeneous production of HNO_3 can be either production or loss of HO_x, depending on the relative rates of reactions R6 and R5.

When the heterogeneous conversion of $NO_2 \rightarrow HNO_3$ occurs, NO_2 is reduced below its gas-phase steady-state concentration and the rates of sequences 4 and 5 are limited by the rate of $OH + NO_2$. Since the primary loss processes for HNO_3 are photolysis and reaction with OH, the rates of these sequences can be expressed as a branching ratio of the photolysis rate, J_{HNO_3}, and the first-order loss rate, $k_{OH+HNO_3}[OH]$. In this case, the rate of sequence 4 is given by the fraction of HNO_3 formed by $OH + NO_2$ that subsequently removes HO_x:

$$r_{S4} = r_{OH+NO_2} \frac{k_{OH+HNO_3}[OH]}{k_{OH+HNO_3}[OH] + J_{HNO_3}} \qquad (2)$$

The rate of the null sequence is the fraction of reaction R5 that subsequently produces OH via reaction R6:

$$r_{S5} = r_{OH+NO_2} \frac{J_{HNO_3}}{k_{OH+HNO_3}[OH] + J_{HNO_3}} \qquad (3)$$

The rate of the heterogeneous removal sequence is equal to the remainder of the total removal rate of OH by HNO_3. The factor of 2 is required for mass balance:

$$r_{S7} = {}^1/_2[r_{OH+HNO_3} - r_{S4}] \qquad (4)$$

The rate of heterogeneous production sequence is completely analogous:

$$r_{S6} = {}^1/_2[r_{HNO_3+h\nu} - r_{S5}] \qquad (5)$$

Note that the eq 3 and eq 4 are not identically equal to the rates of the heterogeneous steps. They are equal to the rate of HO_x production and loss resulting from the NO_2:HNO_3 system not being in steady state. However, since this is mostly a result of the nighttime heterogeneous reactions, these will be referred to as the heterogeneous sequences.

Analogous heterogeneous reactions involving $BrONO_2$ (or $ClONO_2$) + $H_2O \rightarrow$ HOBr (or HOCl) + HNO_3 also convert H_2O to HO_x.[15] Because photolysis of HOBr and HOCl produce OH, the net effect of these sequences is always production of HO_x. These reactions can be significant sources of HO_x at high SZA when production from primary sources is small.[13,16,17]

Pernitric acid, HNO_4, is formed from the reaction of HO_2 and NO_2. The reaction of OH with O_3 is the primary source of HO_2 in the lower stratosphere, with this reaction accounting for ~95% of the HO_2 production in this data set. The sequence that produces and removes HNO_4 also removes HO_x:

$$\begin{aligned} &OH + O_3 \rightarrow HO_2 + O_2 \\ &HO_2 + NO_2 \xrightarrow{M} HNO_4 \\ &OH + HNO_4 \rightarrow H_2O + NO_2 + O_2 \qquad \text{(R7)} \\ &\text{net: } 2OH + O_3 \rightarrow H_2O + 2O_2 \qquad \text{(S8)} \end{aligned}$$

Unlike HNO_3, pernitric acid has no known heterogeneous source. Thus, the concentration of HNO_4 does not vary at night because all sources and sinks of HNO_4 are turned off. Because of this and a significantly shorter photochemical lifetime (~1 day vs ~10 days), HNO_4 is generally at or near (±10%) steady state during mid-day. As a result, the loss of HO_x via HNO_4 can be represented by reaction R7. HNO_4 is also an intermediate in a null sequence similar to S6, but since HNO_4 is in steady state during the day, this sequence can be neglected. Note that HNO_4 is not in steady state near sunrise or sunset. During these conditions, the photolysis of HNO_4 can be a significant source or sink of HO_x.[13]

The remaining significant sink for HO_x is the self-reaction

$$\begin{aligned} &OH + O_3 \rightarrow HO_2 + O_2 \\ &OH + HO_2 \rightarrow H_2O + O_2 \qquad \text{(R8)} \\ &\text{net: } 2OH + O_3 \rightarrow H_2O + 2O_2 \qquad \text{(S9)} \end{aligned}$$

This sequence is the dominant sink for HO_x in the tropics and where the concentrations of HNO_3 and HNO_4 are small. Additional production and loss sequences of HO_x are discussed in Johnston and Podolske,[8] but they are not of quantitative importance in the lower stratosphere.

Production and Loss Rates. The differential equation for HO_x is given by $(d[HO_x]/dt) = P - L$, where production and loss rates are the sum of individual reaction rates, $P = \sum_i P_i$ and $L = \sum_j L_j$. Because $P - L$ is much smaller than the largest term in P and L (i.e. the lifetime of HO_x is short), HO_x is in steady state, $d[HO_x]/dt \approx 0$. The reactions that interconvert HO_2 and OH are significantly faster than the production rate of HO_x; thus the production of any HO_x species is equivalent. It is important to note that (1) HO_x is not conserved—increases in HO_2 do not occur at the expense of OH—and (2) changes in HO_2 relative to OH are dominated by null sequences that are independent of the primary production and loss rates of HO_x. In this data set, the loss of HO_x is almost entirely through reactions involving OH. Thus, the concentration of OH reflects changes in production and loss, and the concentration of HO_2 reflects a combination of these changes and changes in HO_x interconversion rates. For these reasons, it is more straightforward to use measurements of OH to examine our understanding

of the production and loss rates of HO_x. The partitioning of HO_x is discussed separately in Lanzendorf et al.[18]

This analysis uses a highly constrained instantaneous steady-state model to determine the production and loss rates of HO_x. All rates are determined with the measured abundance of chemical species and atmospheric properties, such as *T*, *M*, UV flux, etc., when observations are available. The rate coefficients are taken from the JPL-97 and JPL-00 evaluations.[19,20] Photolysis rates are calculated using the radiative-transfer model described by Prather et al.[21] and absorption cross-sections and quantum yields from the JPL-97 compendium. NO_2 concentrations are determined from the mean of the two available measurements or from a steady-state relation when measurements of NO_2 are not available. The difference between the measured and calculated NO_2 is small (<10%) for this data set.[22] HNO_3 is determined from $HNO_3 = NO_y - NO - NO_2 - HNO_4 - ClONO_2$.

When measurements of certain species are not available, concentrations are determined from steady-state relations or from tracer correlations: $ClONO_2$ is determined from a steady-state relation;[23] HCl is determined by subtracting $[ClONO_2]$ from $[Cl_y]$ determined from an empirical Cl_y-N_2O relation;[24] and CH_4 is inferred from the empirical CH_4-N_2O relation.[5] The HCl and CH_4 determined in this manner are only used to fill in missing data from certain flights and comprise a small fraction of the overall data set. The calculated $ClONO_2$ is used for the entire ASHOE/MAESA data set since measurements are unavailable. The analysis is restricted to SZA < 70° for two reasons: (1) to ensure that longer-lived species that must be calculated (i.e., $ClONO_2$, HNO_4, and H_2CO) are at or near steady state and (2) to avoid the complexity and uncertainty of HO_x sources in sunrise and sunset conditions. This selection criteria exclude data obtained in the Antarctic vortex because SZA > 80° for these data. On the basis of these restrictions, the uncertainties in the concentration of species derived from steady-state relations should be accurately represented by the combined uncertainties of the measurements, rate constant, and photolysis rates used in the calculation. The uncertainties of the individual production and loss terms are summarized in Table 1.

TABLE 1: Uncertainties of Reaction Rates[a]

k[A][B]	$\sigma_{k\ or\ J}$	$\sigma_{[A]}$	$\sigma_{[B]}$	σ_{total}
$k[O(^1D)][H_2O]$	+0.35	+0.42	0.05	+0.55
	−0.25	−0.33		−0.42
$k[O(^1D)][CH_4]$	+0.35	+0.42	0.05	+0.55
	−0.25	−0.33		−0.42
k[OH][CH_4]	+0.24	0.25	0.05	+0.35
	0.19			−0.32
k[Cl][CH_4]	+0.32	0.44	0.05	+0.55
	−0.24			−0.50
J[HNO_3]	+0.42	0.12	−	+0.44
	−0.33			−0.35
k[OH][HNO_3]	+0.30	0.25	0.12	+0.41
	−0.23			−0.35
k[OH][NO_2]	+0.30	0.25	0.10	+0.41
	−0.23			−0.35
k[OH][HNO_4]	+1.72	0.25	+1.6	+2.36
	−0.52		−0.38	−0.69
k[OH][HO_2]	+0.65	0.25	0.30	+0.76
	−0.39			−0.55

[a] All uncertainties in the rate constants are from JPL-97 except k_{OH+NO_2} and k_{OH+HNO_3}, which are from JPL-00. The multiply/divide factors in JPL-97and JPL-00 have been converted to fractional uncertainties for $T = 220$ K and $M = 2 \times 10^{18}$ molecules cm^{-3}. The uncertainties in derived species, e.g. $O(^1D)$, include the uncertainties of measurements, photolysis rates, and rate constants used in their determination. Uncertainties in photolysis rates include an additional uncertainty of 0.3 to account for uncertainties in the radiative transfer code and the slant column of O_3. All uncertainties are added in quadrature.

Results

In this analysis, the production and loss rates are calculated independently, so the agreement of *P* and *L* is an indication of how well the system is described. Overall, production and loss are well-balanced, with an average value and standard deviation of $P/L = 1.03 \pm 0.22$, indicating that the production and loss terms adequately describe the HO_x system in general. Nevertheless, there are systematic discrepancies that are concealed within this average. For example, there is a discrepancy between the ASHOE/MAESA and POLARIS data sets: for ASHOE/MAESA, $P/L = 1.1 \pm 0.2$, and for POLARIS, $P/L = 0.8 \pm 0.1$. Some of the difference is possibly a result of the method used to infer the O_3 column above the ER-2. The photolysis rates in the ASHOE/MAESA data set were determined with overhead O_3 columns inferred from TOMS satellite measurements, while the rates in the POLARIS data set were constrained by remote observations obtained in situ aboard the ER-2. In the POLARIS data set, where both methods of determining the O_3 column above the ER-2 are available, differences of 20% between $J_{O(^1D)}$ determined with the two inferred O_3 columns are common.

Another difference in the two data sets is the greater importance of HNO_4 in the POLARIS data set. The concentration of HNO_4 is not measured, and the uncertainty in the reaction rates and absorption cross-sections used to calculate $[HNO_4]$ is large (see Table 1). The uncertainty in the JPL-97 recommended photolysis rate is a factor of 2. Sunrise and sunset measurements of HO_x are consistent with an increase of 1×10^{-5} s^{-1} in the photolysis rate of HNO_4, independent of SZA during daytime.[13] Also, the effects of the uncertainty in the equilibrium constant becomes significant in the high-latitude summer when temperatures are high. For typical conditions experienced at latitudes > 60° N, $T = 225$ *K* and $M = 2 \times 10^{18}$ molecules cm^{-3}, the JPL-97 recommended equilibrium constant for the thermal decomposition of HNO_4 is uncertain by a factor of 15. Using the low uncertainty limit for K_{eq} in the steady-state calculation results in an 80% reduction in $[HNO_4]$. Because of these and other discrepancies, the overall agreement of *P* and *L* should be taken as a figure of merit necessary to interpret the results of this analysis, not as an indication that the photochemistry of HO_x is entirely understood.

HO_x in Continuous Sunlight. The simplest case of HO_x photochemistry occurs in continuous sunlight where the rates of the heterogeneous sequences are negligible. Figure 4 shows the relation of the production rate of HO_x with the product of $J_{O(^1D)}$ and $[O_3]$ for observations made in continuous sunlight (24 h day) during POLARIS. The product $J_{O(^1D)} \times [O_3]$ is equal to the rate of the initiation step in sequences 1 and 2, not the rate limiting steps. The correlation is tight for a number of reasons. First, the primary sink of $O(^1D)$ is quenching by O_2 and N_2 into the ground-state atom, $O(^3P)$. Thus, the removal of $O(^1D)$ is independent of the chemical composition of the lower stratosphere and its abundance is proportional to $J_{O(^1D)} \times [O_3]$. Second, the concentrations of the source gases H_2O and CH_4 that determine the rates of HO_x production are nearly constant, $[H_2O] = (9.4 \pm 1.0) \times 10^{12}$ and $[CH_4] = (2.5 \pm 0.4) \times 10^{12}$ molecules cm^{-3}. Third, the rates of the sequences that involve CH_4 are also proportional to J_{H-CHO} and OH; both strongly correlate with $J_{O(^1D)}$. Thus, the changes in HO_x production are driven almost entirely by changes in O_3 and photolysis rates. The result is a remarkably tight correlation between the

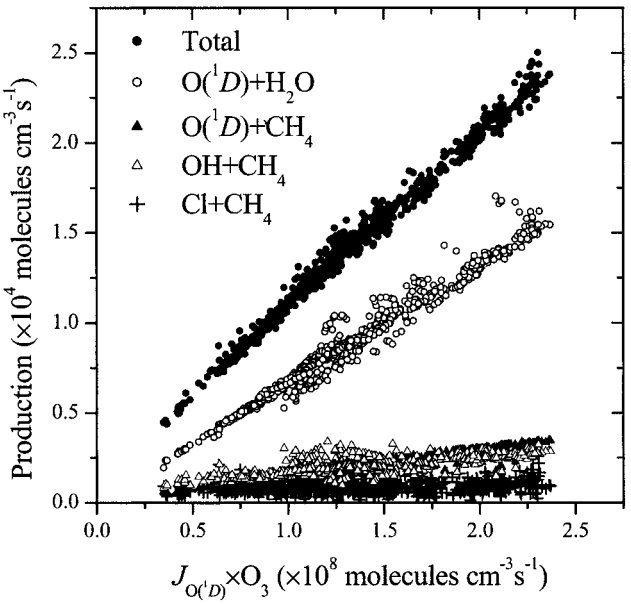

Figure 4. Individual and total production rates of HO_x versus the production rate of $O(^1D)$, $J_{O(^1D)}\times[O_3]$. The data are restricted to $M < 2.5 \times 10^{18}$ molecules cm^{-3}, SZA < 70°, and to air parcels exposed to solar illumination for more than 90% of the time for the 5 days prior to observation.

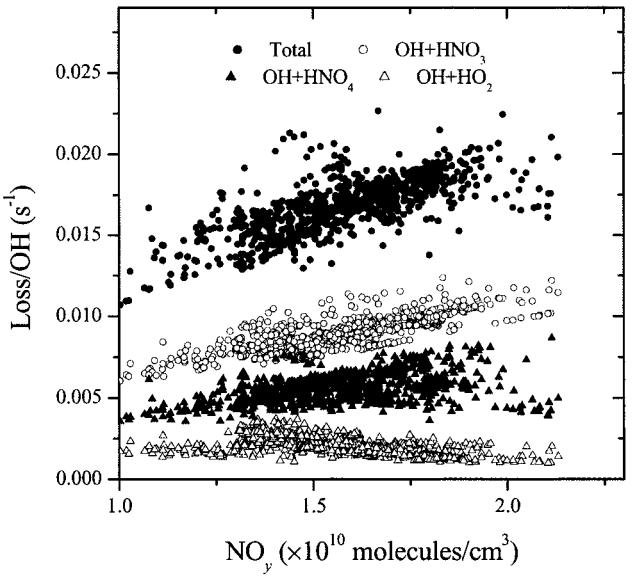

Figure 5. Individual and total first-order loss rates of HO_x versus $[NO_y]$. The SZA dependence of the rates is removed by dividing by OH. The data are restricted to $M < 2.5 \times 10^{18}$ molecules cm^{-3}, SZA < 70°, and to air parcels exposed to solar illumination for more than 90% of the time for the 5 days prior to observation.

production rate and $J_{O(^1D)}\times[O_3]$. This correlation is not restricted to continuous sunlight. A similar relation is obtained for all data in this data set.

The loss rates for observations in continuous sunlight are shown in Figure 5. Because of the absence of heterogeneous chemistry in these data, the NO_2:HNO_3 system is at or near (within 20%) steady state. The loss from sequence 4 is represented by the rate limiting step, OH + HNO_3. The loss rates show a fairly good correlation with NO_y, but this correlation is not nearly as tight as that seen in Figure 4 for the production terms. The loss rates are proportional to NO_y because HNO_3 and HNO_4 correlate and HO_2 anticorrelates with NO_y. It is tempting to conclude that the processes that control OH are proportional to O_3 and NO_y and that OH can be described by a

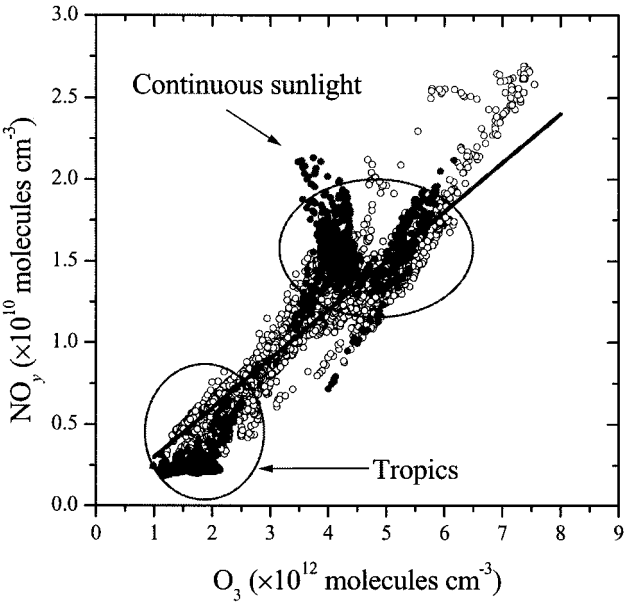

Figure 6. O_3 and NO_y obtained during ASHOE/MAESA and POLARIS for $M < 2.5 \times 10^{18}$ molecules cm^{-3} and SZA < 70°. Data obtained during continuous sunlight and in the tropics are highlighted. The line represents the average value, $O_3/NO_y \approx 335$.

simple relation, $[OH] \propto J_{O(^1D)}\times[O_3]/[NO_y]$. It is also tempting to conclude that [OH] is a nearly constant function of SZA because O_3 and NO_y generally correlate within the lower stratosphere. However to do so would neglect the chemistry that controls the production and loss of HO_x when this correlation breaks down.

Figure 6 shows the correlation of O_3 and NO_y for all latitudes. The data obtained in continuous sunlight, corresponding to the data in Figures 4 and 5, are highlighted for reference. For most of the data O_3 and NO_y are correlated. On average $O_3/NO_y = 335 \pm 125$, but this ratio ranges from 200 to 400 in mid-latitudes and can reach 1000 in the tropics.[25] The data in continuous sunlight are not particularly well-correlated. At a given $[O_3]$, $[NO_y]$ changes by a factor of 2, yet changes of this magnitude are not observed in the OH data. Clearly, there is another process in addition to the absolute abundance of NO_y that controls the loss rate of HO_x.

In continuous sunlight, the partitioning of NO_y between NO, NO_2, HNO_3, and HNO_4 is controlled by O_3 and HO_x. The concentrations of NO_x, HNO_3, and HNO_4 normalized to NO_y and the concentration of HO_2 normalized to OH are shown versus O_3/NO_y in Figure 7a. Also shown is the expected trend calculated from steady-state relations using the median values of photolysis rates, rate constants, and chemical concentrations of the data shown in Figures 4 and 5, with the exception of $[O_3]$, which is varied between 2×10^{12} and 8×10^{12} molecules cm^{-3}. For this calculation $[OH] = 1.2 \times 10^6$ molecules cm^{-3} and $[NO_y] = 1.5 \times 10^{10}$ molecules cm^{-3}. As a result, the calculation shows how the partitioning of a fixed amount of NO_y changes with increasing O_3. For these data $[NO_2]/[NO]$ is proportional to O_3; $[HO_2]/[OH]$ is proportional to $[O_3]$ and inversely proportional to [NO]; $[HNO_3]$ is proportional to [OH] and $[NO_2]$; and $[HNO_4]$ is proportional to $[HO_2]$ and $[NO_2]$. As O_3 increases, the partitioning of NO_y is driven toward the higher oxides of nitrogen that remove HO_x. At the same time higher O_3 (and lower NO_x) results in higher concentrations of HO_2.[18] Note that unlike NO_y, HO_x is not conserved; i.e., HO_2 does not increase at the expense of OH. Thus, for a fixed amount of NO_y, an increase in O_3 results in increased loss rates.

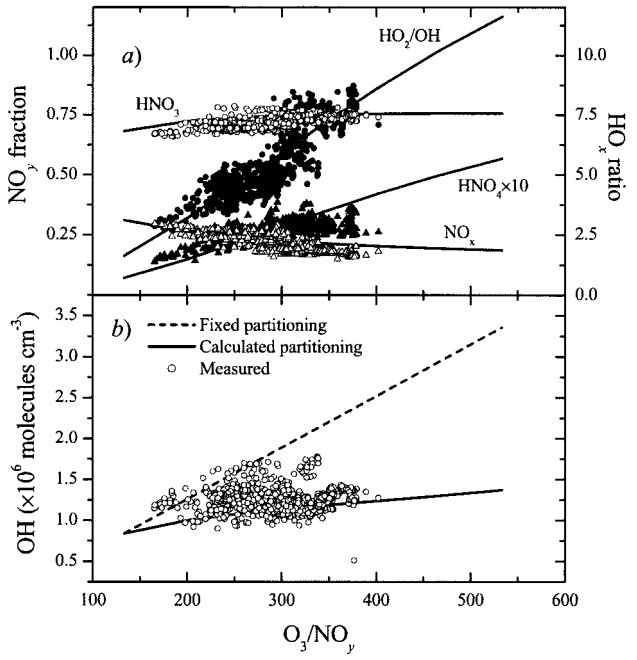

Figure 7. (a) Observed and calculated partitioning of NO_y (left ordinate) and HO_2/OH (right ordinate) versus O_3/NO_y. The lines are calculated from median values of the parameters used to calculate the production and loss rates shown in Figures 4 and 5 (*e.g.* $NO_y = 1.5 \times 10^{10}$ molecules cm^{-3}, $J_{O(^1D)} = 3 \times 10^{-5}$ s^{-1}, $T = 229$ K, ...). The concentration of O_3 is varied between 2×10^{10} and 8×10^{10} molecules cm^{-3}. The fraction HNO_4/NO_y is multiplied by 10 in the figure. (b) Calculated and observed OH versus O_3/NO_y. The solid line is determined using the calculated concentrations shown by the lines in a. The dashed line represents the OH obtained with the calculated concentrations determined at $O_3 = 2 \times 10^{10}$ molecules cm^{-3}. The measured data are normalized to SZA = 55° using the fit in Figure 1.

Figure 7b shows the effects of partitioning on the calculated concentration of OH. The concentration of OH is calculated with the median values of the production terms from Figure 4 (except for O_3) and the loss rates determined from the calculated concentrations of HNO_3, HNO_4, and HO_2 shown in Figure 7a. Also shown is the OH calculated with the concentrations of HNO_3, HNO_4, and HO_2 held constant to the values determined at $O_3 = 2.0 \times 10^{12}$ molecules cm^{-3}, the low end of the range in O_3. The observed OH is normalized by the fit in Figure 1 and multiplied by the median value of OH. The underestimate of OH by 25% is typical of all data within the POLARIS data set and is not restricted to the limit of continuous sunlight. The large difference between the two model curves represents the effect of the partitioning of the loss terms on the total loss rate. With the concentrations of the loss terms held constant (i.e. the first-order loss rate is constant) the calculated concentration of OH increases by a factor of 4 with this 4-fold increase in O_3. This reflects the nearly linear dependence of the production rate of HO_x on $[O_3]$ (Figure 6). However, as shown in Figure 7a, there is a 7-fold increase in $[HO_2]$ and a factor of 4 increase in $[HNO_4]$. Since these species contribute roughly 50% of the gas-phase removal rate of HO_x (Figure 5), the model that includes these changes shows only a small change in the calculated concentration of OH.

The relationships between the production rate of HO_x with the product of $J_{O(^1D)}$ and $[O_3]$ shown in Figure 4 and of the loss rate with $[NO_y]$ shown in Figure 5 form the basis for understanding the factors that regulate HO_x. The production of HO_x is described by a small number of similar terms dominated by the production of $O(^1D)$. This and the smaller contribution from the branching ratio for the photolysis of H_2CO determine

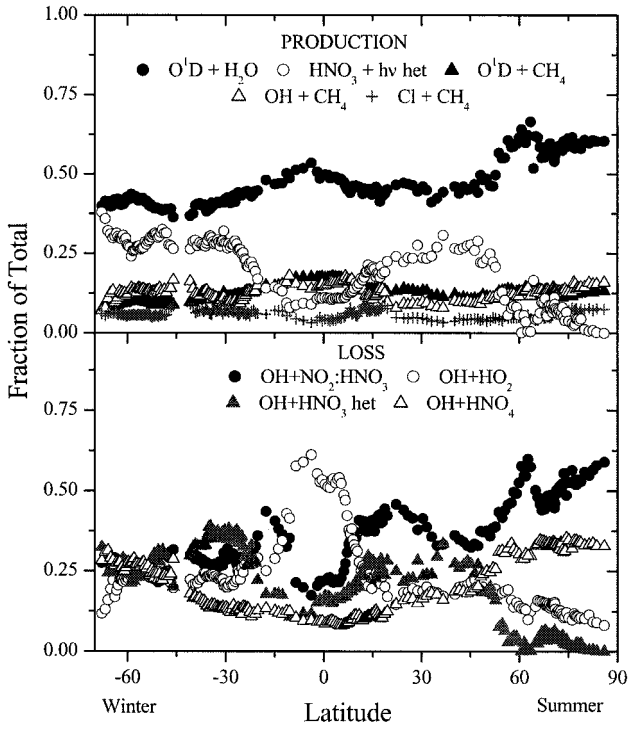

Figure 8. Fractional (a, top) production and (b, bottom) loss rates of HO_x versus latitude. The data are restricted to SZA < 70° and $M < 2.5 \times 10^{18}$ molecules cm^{-3} and averaged into bins of latitude using 20 data points per bin. OH + NO_2:HNO_3 refers to sequence 4, the gas-phase NO_2-HNO_3 removal sequence The data at high northern latitudes were obtained predominantly in summertime, and those in the southern high latitudes were obtained predominantly in wintertime.

the shape of the diurnal change of OH. The loss of HO_x is described by only three reactions, all of them involving species that are proportional to OH, O_3, and NO_y. The correlation between O_3 and NO_y can generally result in the cancellation in changes in production and loss rates. The correlation does not have to be perfect because repartitioning of the loss terms buffers the system against changes in O_3/NO_y. Though this example is restricted to continuous sunlight where the calculation is simple, the interpretation of the effects of repartitioning in NO_y and HO_x due to changes in O_3/NO_y is applicable throughout this data set. The introduction of heterogeneous reactions should be viewed as a perturbation to this basic system.

Role of HNO_3. The production rate of HO_x is shown versus latitude in Figure 8a. The data are restricted to SZA < 70° and averaged in bins of latitude, with each data point representing a 20 min average. The result reflects the sampling of the ASHOE/MAESA and POLARIS missions: the Southern hemisphere data are predominantly winter, and the Northern hemisphere data are predominantly summer. The data shown in Figures 4 and 5 are limited to latitudes above 70° N and comprise less than 10% of the overall data set. For most of the lower stratosphere the production of HO_x from the photolysis of HNO_3 following the heterogeneous production of HNO_3 is a large fraction of the total production rate. The drop in production from the photolysis of HNO_3 in latitudes between 20° S and 10° N reflects the change in O_3/NO_y observed in the tropics.[25] The fractional contributions of other species is fairly constant, a result of the nearly constant concentrations of the source gases in the lower stratosphere. In this data set, the average concentrations are $[H_2O] = (9.4 \pm 0.9) \times 10^{12}$ and $[CH_4] = (2.7 \pm 0.5) \times 10^{12}$ molecules cm^{-3}.

The loss terms of HO_x are shown versus latitude in Figure 8b. The gas-phase removal of OH by sequence 4, denoted OH

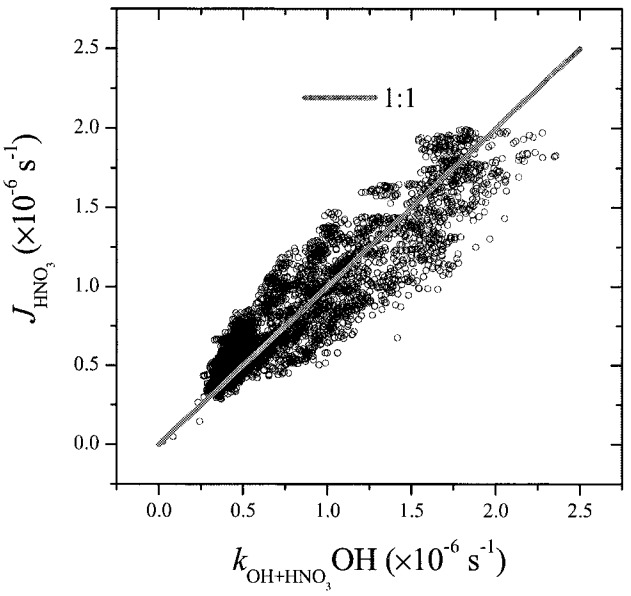

Figure 9. First-order rates of HNO_3 removal via photolysis, J_{HNO_3}, and reaction with OH, k_{OH+HNO_3}[OH], plotted versus each other for all data at $M < 2.5 \times 10^{18}$ molecules cm^{-3} and SZA < 70°.

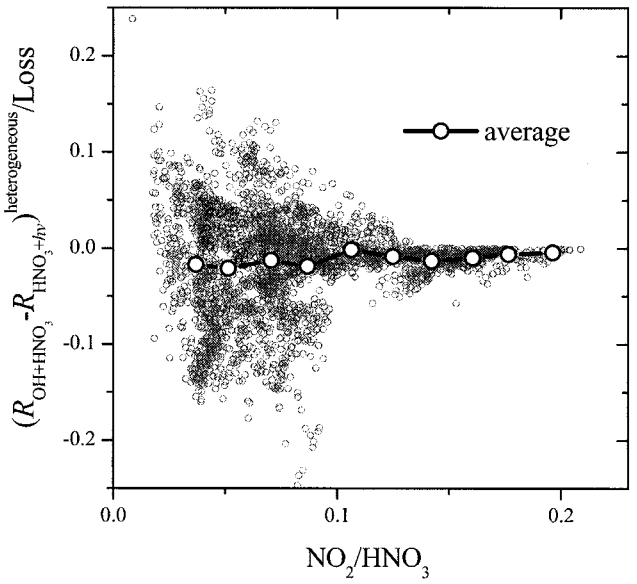

Figure 10. Difference between the heterogeneous loss and production sequences normalized to the total loss rate of HO_x versus NO_2/HNO_3 for all data at $M < 2.5 \times 10^{18}$ molecules cm^{-3} and SZA < 70°. The average value of this fraction is also shown.

+ NO_2:HNO_3, dominates the loss of HO_x in the summertime where the rate of the heterogeneous removal is smallest and concentrations of NO_2 are largest. Similar to the heterogeneous production sequence, the removal of HO_x by HNO_3 via the heterogeneous sequence becomes a large component of the loss rate outside of regions in continuous sunlight. In the tropics, the removal by OH + HO_2 dominates because of the large decrease in NO_y observed at those latitudes. There is more variability in the fractional contributions of the loss terms compared to the production terms, reflecting the combined effects of changes in the partitioning of NO_y resulting from heterogeneous conversion of $NO_2 \rightarrow HNO_3$ and from changes in the O_3/NO_y in the tropics.

The heterogeneous conversion of $NO_2 \rightarrow HNO_3$ impacts OH in three ways: (1) enhancing production, (2) enhancing loss, and (3) reducing the rate of sequence 4 by reducing NO_2. The first two are coupled and can be examined together. The relative production and loss of HO_x from the heterogeneous sequences is determined by the branching ratio of the removal of HNO_3 through photolysis versus reaction with OH (see Figure 3). This branching ratio is defined by the relative magnitudes of first-order loss rates, J_{HNO_3} and k_{OH+HNO_3}[OH]. Figure 9 shows the relation between these two pathways for all data at SZA < 70°. The correlation is expected, since OH and J_{HNO_3} correlate with UV flux. However, the near equality is surprising since there is no direct link between k_{OH+HNO_3}[OH] and the photolysis rate of HNO_3.

As a result of $k_{OH+HNO_3}[OH] \approx J_{HNO_3}$, the branching ratios of the heterogeneous production and loss sequences are nearly equal,

$$\frac{J_{HNO_3}}{k_{OH+HNO_3}[OH] + J_{HNO_3}} \approx \frac{k_{OH+HNO_3}[OH]}{k_{OH+HNO_3}[OH] + J_{HNO_3}} \quad (6)$$

and the net effect of the heterogeneous sequences on HO_x is negligible. This is shown in Figure 10 for all data at SZA < 70°. The difference between the heterogeneous production and loss sequences is normalized to the total loss rate and plotted versus NO_2/HNO_3, which is inversely proportional to the rates of the heterogeneous sequences. The net contribution of the heterogeneous rates is largest at the lowest NO_2/HNO_3 values where the heterogeneous rates are fastest. However, the difference rarely exceeds 10% of the overall rate, and on average is zero with a standard deviation of 0.04.

The net effect of all of the HNO_3 sequences on OH is essentially equal to the rate of sequence 4. Thus, the net production terms of HO_x are nearly identical to those shown in Figure 4. Likewise, the loss terms resemble those in Figure 5, but with one notable exception. In the case in which there is heterogeneous conversion of $NO_2 \rightarrow HNO_3$, the loss rate of sequence 4 is controlled by NO_2, not by HNO_3 as was the case in continuous sunlight. Though the heterogeneous production of HNO_3 has no direct effect on OH, it has an indirect effect through the removal of NO_2. This can be seen in eq 2: since $k_{OH+HNO_3}[OH] \approx J_{HNO_3}$, the changes in the rate of HO_x loss by sequence 4 are driven entirely by the changes in r_{OH+NO_2} and, hence, changes in NO_2/HNO_3 driven by the heterogeneous conversion of $NO_2 \rightarrow HNO_3$.

When the contributions of the heterogeneous sequences to the production and loss rates are removed, the effect of heterogeneous conversion of $NO_2 \rightarrow HNO_3$ on the loss rates can be examined. Figure 11 shows the production and loss rates of the remaining terms plotted versus NO_2/HNO_3 for $[HNO_3] = (1.1 \pm 0.2) \times 10^{10}$ molecules cm^{-3}, $[O_3] = (4.5 \pm 1.0) \times 10^{12}$ molecules cm^{-3} and SZA < 70°. In this case O_3 is held constant in order to separate the effects of O_3 from those of heterogeneous chemistry on the partitioning of NO_y. The SZA dependence of the production and loss rates is removed by dividing by OH. The production terms are nearly constant because $[O_3]$ is held constant. The change in rate of $O(^1D)$ + H_2O reflects the change in the photolysis rate of O_3 ($J_{O(^1D)}$) resulting from changing overhead ozone (Figure 11a).

The loss rates are also tight functions of NO_2/HNO_3. The loss rates R_{OH+HNO_4} and R_{OH+HO_2} are very compact in relation to NO_2/HNO_3 because $[HNO_4]$ correlates and $[HO_2]$ anticorrelates with $[NO_2]$. For constant $[O_3]$, $[HO_2]$ is inversely proportional to $[NO_2]$;[18] thus, R_{OH+HO_2} decreases with increasing NO_2/HNO_3. However, the change in the loss rate due to HO_2 only partially offsets the change in the rate of sequence 4. At constant SZA, the concentration of HNO_4 is proportional to the

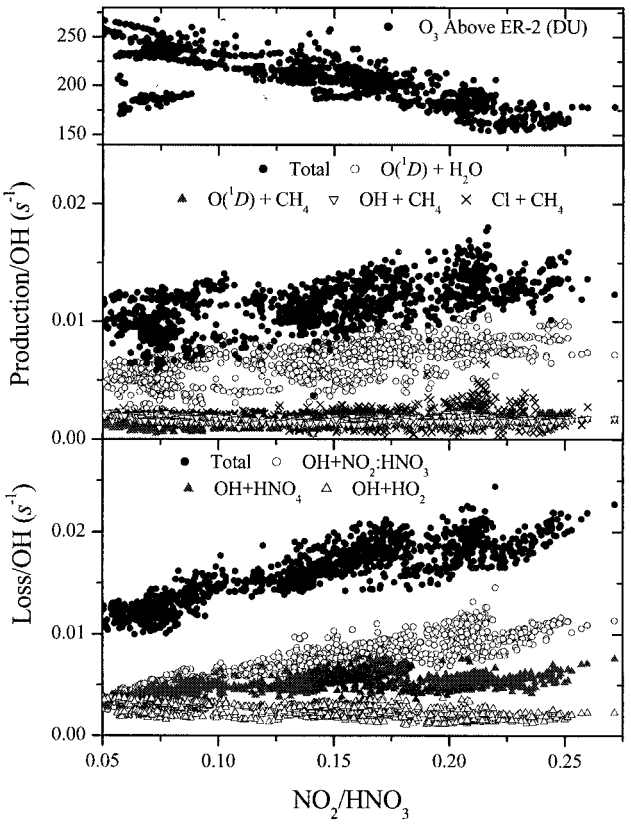

Figure 11. O_3 column above the ER-2 and the net production and loss rates of HO_x versus NO_2/HNO_3. The heterogeneous production and loss sequences of HNO_3 have been removed from the total rates. These data are selected for $[HNO_3] = (1.1 \pm 0.2) \times 10^{10}$ molecules cm^{-3}, $[O_3] = (4.5 \pm 1.0) \times 10^{10}$ molecules cm^{-3}, SZA < 70°, and $P/L = 0.85 \pm 0.15$.

product of $[HO_2]$ and $[NO_2]$. Thus, the change in the loss of HO_x due to HNO_4 is more moderate than that of sequence 9. The net effect of the changes in the loss rates of HO_x due to changes in $[HO_2]$ and $[HNO_4]$ is small. The increase in the loss rate of HO_x due to sequence 4 is not offset by changes in the other loss terms but by the coincident increase in production rates due to decreased overhead O_3.

The anticorrelation between NO_2/HNO_3 and overhead O_3 dampens the effect of the change in the rate of sequence 4 on [OH]. However, even if this anticorrelation were not observed, the net perturbation to OH would be small. The net loss rate shown in Figure 11 changes by only 50% between $NO_2/HNO_3 = 0.05$ and 0.25 even though sequence 4 increases by a factor of 4 or 5. Expressed as a fraction, the net loss rate is constant to within ±20% of the mean. This is because sequence 4 contributes only 30−50% of the net loss without the heterogeneous removal sequence included. These data have been selected to obtain the greatest dynamic range in the perturbation to the loss rate of HO_x, yet the net loss rate is constant to within ±20%. The same trend in the loss rates is seen with any constant $[HNO_3]$ because the abundances of the other loss terms (HNO_4 and HO_2) are influenced by the partitioning of NO_y. In the absence of some external perturbation, such as polar processing of chlorine compounds or denitrification, there will not be a significant departure from the correlations shown in Figure 11.

The anticorrelation between the O_3 column and NO_2/HNO_3 shown in Figure 11 is not generally observed. This correlation results from the coincidence of the annual summertime decline in the high-latitude O_3 column with the decrease in heterogeneous conversion of $NO_2 \rightarrow HNO_3$ resulting from near continuous daylight. In general, the O_3 column does not correlate with the partitioning of NO_y, and it is the only parameter that consistently correlates with the deviation of the concentration of OH from the fit shown in Figure 1. This trend is driven by the strong dependence of $J_{O(^1D)}$ and J_{H-HCO} on the overhead O_3 column and the resulting change in production rates. This trend also correlates with altitude, and hence pressure, temperature, etc. There is a slight asymmetry between am and pm in the difference between the fit and the data in Figure 1 due to changes in overhead O_3. The ER-2 generally departs in the morning and returns in the afternoon. The return leg is usually at a higher altitude and lower overhead O_3, resulting in 5% higher OH on average in the afternoon compared to morning in this data set.

OH in the Tropics. The relative magnitudes of the production and loss terms of HO_x in the tropics, roughly 10° S to 10° N in Figure 8, are distinctly different from those in the mid- and high-latitudes. The primary difference is the smaller concentration of NO_y relative to O_3, resulting in a smaller fractional contribution of the HNO_3 sequences. The description of the production of HO_x in the tropics is thus greatly simplified. The production of HO_x is dominated by the oxidation of H_2O and CH_4, with these sequences accounting for roughly 85% of the total production rate.

The description of the loss terms is more complicated. The reaction of OH with HO_2 accounts for roughly 40% of the total removal rate, but there are significant contributions from the other removal mechanisms. Though the role of HNO_3 in the removal of HO_x is smaller in the tropics, the simplifying characteristics discussed in the previous section still hold. The cancellation of the heterogeneous production and loss sequences reduce the net removal rate of HO_x from the four sequences involving HNO_3 to approximately the rate of removal by sequence 4, identical to the previous discussion. However, there is an additional simplifying condition in the tropics because the lack of seasonal variability in the length of day precludes large changes in NO_2/HNO_3, and hence, changes in the rate of sequence 4. For tropical data, this ratio is essentially constant: $NO_2/HNO_3 = 0.1 \pm 0.01$.

Figure 12 shows how the net loss rates respond to changes in O_3 and to the partitioning of NO_2/NO and HO_2/OH. The data are selected for $[HNO_3] = (1.5 \pm 0.3) \times 10^9$ molecules cm^{-3}, SZA < 70°, albedo < 0.4, and $[O_3]/[HNO_3] > 650$. The restriction on $[HNO_3]$ limits variability in the loss terms and the restriction on O_3/NO_y limits the data to observations in the tropics. The restriction on albedo reduces scatter introduced by higher photolysis rates: the anomalously high concentrations of OH in Figure 1 at SZA ~ 25° correspond to observations above high tropical clouds where the UV reflectivity is high. In this region the self-removal mechanism, sequence 9, dominates the removal of HO_x. This results from the large decrease in the concentrations of NO_y species, not because of an increase in HO_2. In fact, the HO_2/OH ratio is observed to be lowest in the tropics where O_3 concentrations are low, because the reaction $OH + O_3$ is the primary source of HO_2.

The primary perturbation in the loss rate of HO_x in the tropics is observed in the rate of $OH + HO_2$. A consequence of the constant NO_2/HNO_3 and the restriction of the data to a constant $[HNO_3]$ is that changes in the concentration of HO_2 are driven directly and indirectly by changes in O_3. Increased O_3 increases HO_2 production from OH. At the same time, reaction with O_3 converts NO to NO_2, decreasing the conversion rate of HO_2 to OH by reaction with NO. As a result, increases in O_3 lead to increased loss rates through $OH + HO_2$. Since the NO_2-HNO_3 system is constant, changes in both production and loss rates

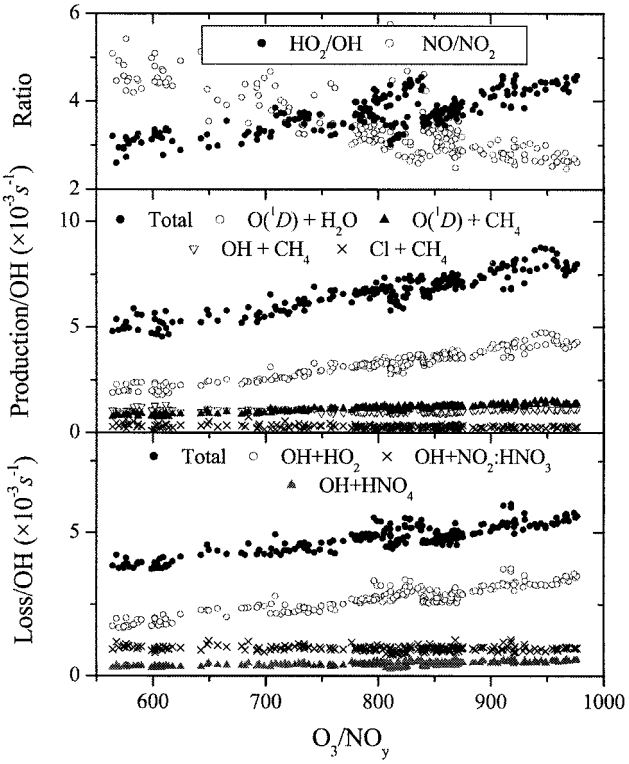

Figure 12. Ratios of NO/NO_2 and HO_2/OH and the net production and loss rates of HO_x in the tropics versus O_3. The heterogeneous production and loss sequences of HNO_3 have been removed from the total rates. These data are selected for $[HNO_3] = (1.5 \pm 0.3) \times 10^9$ molecules cm^{-3}, SZA < 70°, and albedo < 0.4.

are driven entirely by changes in O_3. The other loss terms are small and essentially constant, so that the change in the loss rate is offset by the corresponding change in the production rate, similar to the case of continuous sunlight.

Summary and Conclusions

The remarkable relation of OH and UV flux, represented by SZA in Figure 1, belies the complexity of the HO_x system. The large number of reactions that result in production and loss of HO_x precludes a simple explanation for this relation. However, the use of rate limiting steps in reaction sequences greatly simplifies how we think of the HO_x system. Instead of dozens of sources and sinks of HO_x, there are only a few: HO_x is produced from O_3, H_2O, and CH_4 and removed by NO_y and HO_x. In general, the production rate of HO_x is proportional to O_3 and UV flux and the loss rate is proportional to NO_y. The invariability of H_2O and CH_4 and the correlation of O_3 and NO_y, combined with control of the partitioning of NO_y by O_3 and HO_x, form the basis for the invariability of OH within this data set.

The breakdown of this simple generality occurs with the introduction of the heterogeneous conversion of $NO_2 \rightarrow HNO_3$. The heterogeneous repartitioning of NO_y is significant for two reasons: (1) Heterogeneous production of HNO_3 results in production and loss of HO_x; and (2) the conversion of $NO_2 \rightarrow HNO_3$ results in significantly smaller loss rates for HO_x. In both cases, other processes act to negate the effects of this repartitioning. The production of HO_x from HNO_3 generated by heterogeneous reactions is offset by a nearly identical removal rate. The net effect is that the heterogeneous production of HNO_3 has little direct impact on OH concentrations. In the second case, the enhanced loss rates at high NO_2/HNO_3 are offset by increased photolysis rates resulting from the decreased O_3 column above the ER-2. The net effect is that OH concentrations are not significantly reduced.

In the tropics, the correlation between O_3 and NO_y changes, and the fractional contribution of NO_y to the production and loss rates decreases. Because of the lesser role of NO_2 and HNO_3, the changes in the production and loss rates are driven mostly by changes in O_3 and HO_2, similar to the limit of continuous sunlight where heterogeneous rates are negligible. The changes naturally compensate, and the net effect on the observed abundance is small. In both the tropics and the higher latitudes, these perturbations are small fractions of the total production and loss rate.

The prominent role played by reactive nitrogen in the HO_x photochemistry presented here is partly a result of the observation strategy of the POLARIS mission. The mission was designed to obtain measurements during the period that NO_x controls ozone loss rates; hence, a large dynamic range of NO_x/NO_y measurements is available for analysis. The effect of chlorine partitioning on HO_x has not been addressed in detail, but it should play a significant role in the production and loss rates of HO_x. The few measurements of OH in the Antarctic winter polar vortex show that concentrations of OH are highly variable and strongly dependent on chlorine partitioning.[17] Other perturbations within the vortex, such as dehydrification, denitrification, and decreased CH_4, are also likely to have some effect on OH abundances. Extensive measurements of OH in the winter Arctic vortex have been obtained in the SOLVE (SAGE III Ozone Loss Validation Experiment) campaign in the winter of 2000 and will be discussed in forthcoming papers.

Acknowledgment. We thank the pilots and crew of the NASA ER-2 and the logistical support of NASA AMES. This work was supported by the NASA Upper Atmospheric Research Program and the Atmospheric Effects of Aviation Project.

References and Notes

(1) Wennberg, P. O., et al., *Science* **1994**, *266*, 398.
(2) Fahey, D. W. et al., *Geophys. Res. Lett.* **2000**, *27*, 2605.
(3) Salawitch, R. J., et al., *Science* **1993**, *261*, 1146.
(4) Sen, B, et al. *J. Geophys. Res.* **1999**, *104*, 26, 653−26, 665; Gao, R. S., et al., *J. Geophys. Res.* **1997**, *102*, 3935.
(5) Herman, R. L., et al. *Chemosphere: Global Change Science* **1999**, 1, 173.
(6) Perkins, K. K., et al. *J. Phys. Chem. A*, this issue.
(7) Voss, P. B., et al., *J. Geophys. Res., in press*.
(8) Johnston, H. S.; Podolske, J. R. *Rev. Geophys. and Space Phys.* **1978**, *16*, 491.
(9) Johnston, H. S.; Kinnison, D. *J. Geophys. Res.* **1998**, *103*, 21967.
(10) Tuck, A. F.; Brune, W. H.; Hipskind, R. S. *J. Geophys. Res.* **1997**, *102*, 3901.
(11) A brief description of the aircraft measurement capability is described by Newman, P. A.; Fahey, D. W.; Brune, W. H.; Kurylo, M. J.; Kawa, S. R. *J. Geophys. Res.* **1999**, *104*, 26481. Complete descriptions of individual instruments are given by references within.
(12) Wennberg, P. O.; Cohen, R. C.; Hazen, N. L.; Lapson, L. B.; Allen, N. T.; Hanisco, T. F.; Oliver, J. F.; Lanham, N. W.; Demusz, J. N.; Anderson, J. G. *Rev. Sci. Instr.* **1994**, *65*, 1858.
(13) Wennberg, P. O., et al., *Geophys. Res. Lett.* **1999**, *26*, 1373.
(14) Pickett, H. M.; Peterson, D. B. *J. Geophys. Res.* **1996**, *101*, 16789.
(15) Hanson, D. R.; Ravishankara, A. R. *J. Phys. Chem.* **1993**, *97*, 28023; *J. Geophys. Res*. **1991**, 96, 5081.
(16) Lary, D. J.; Chipperfield, M. J.; Toumi, R.; Lenton, T. *J. Geophys. Res.* **1996**, *101*, 1489.
(17) Jaeglé, L., et al. *J. Geophys. Res.* **1997**, *102*, 13235.
(18) Lanzendorf, E. J.; Hanisco, T. F.; Wennberg, P. O., Cohen, R. C.; Stimpfle, R. M.; Anderson, J. G.; Gao, R. S.; Margitan, J. J.; Bui, T. P. *J. Phys. Chem A.*, this issue.
(19) DeMore, W. B.; Sander, S. P.; Golden, D. M.; Hampson, R. F.; Kurylo, M. J.; Howard, C. J.; Ravishankara, A. R.; Kolb, C. E.; Molina, M. J. *Chemical Kinetics and photochemical data for use in stratospheric modeling, Evaluation number 12*, JPL Publication 97-4, Jet Propulsion Laboratory, 1997.

(20) Sander, S. P.; Friedl, R. R.; DeMore, W. B.; Golden, D. M.; Kurylo, M. J.; Hampson, R. F.; Huie, R. E.; Moortgart, G. K.; Ravishankara, A. R.; Kolb, C. E.; Molina, M. J. *Chemical Kinetics and photochemical data for use in stratospheric modeling, Supplement to Evaluation number 12*, JPL Publication 00-3, Jet Propulsion Laboratory, 2000.
(21) Prather, M. J. *J. Geophys. Res.* **1981**, 86, 5325.
(22) Del Negro, L. A. et al., *J. Geophys. Res.* **1999**, *104*, 26687.
(23) Stimpfle, R. S. et al., *J. Geophys. Res.* **1999**, *104*, 26705.
(24) Bonne, G. P. et al. *J. Geophys. Res.* **2000**, *105*, 1957.
(25) Fahey, D. W., et al., *Geophys. Res. Lett.* **1996**, *23*, 1653.